

## Electron temperature and density dependence of $E1$ and $E2$ lines in the spectra of cobaltlike to potassiumlike ions

K. B. Fournier\* and W. H. Goldstein

*Lawrence Livermore National Laboratories, P.O. Box 808, Livermore, California 94550*

M. May and M. Finkenthal†

*Department of Physics and Astronomy, The Johns Hopkins University, Baltimore, Maryland 21218*

(Received 13 September 1995)

We report on a model for the intensity of “forbidden”  $3d^k-3d^{k-1}4s$  electric quadrupole ( $E2$ ) transitions in ions with ground states of the form  $3p^63d^k$  ( $k=1$  through 9) across a broad range of temperatures and densities. (Molybdenum,  $Z=42$ , has been chosen as a representative element because of its role in magnetically confined fusion experiments and the availability of experimental data.) We make an identification of a  $3d^8-3d^74s$   $E2$  line in Mo XVII. In ions where strong  $E2$  lines are not seen (ions with ground states  $3d^k$ ,  $1 \leq k \leq 7$ ), the suppression of the lines is explained by dipole decays to low-lying levels other than the ground state that become allowed through configuration interaction between  $3d^{k-1}4s$  states and excited states that have electric dipole ( $E1$ ) decays to the  $3p^53d^{k+1}$  levels (and in like manner mixing between the  $3p^53d^{k+1}$  configuration and other configurations with  $E1$  decays to the levels of  $3d^{k-1}4s$ ). For  $k=8$  and 9, we find that radiative cascades from high-lying levels play an important role in populating upper states of the  $E2$  transitions. The role of direct, collisional ionization from valence and inner subshells of adjacent charge states in populating the upper states of  $3d-4p$   $E1$  and  $3d-4s$   $E2$  decays in Mo XVI and Mo XVII is found to be negligible. General agreement is found between observations of the  $E2$  to  $E1$  brightness ratio of Mo XVI made in a tokamak plasma and the predictions of the present model. Sensitivity to changes in electron density in the ratio of  $E2$  to  $E1$  decays can be used as a diagnostic for fusion plasmas.

PACS number(s): 32.70.Fw, 52.25.Vy, 31.15.Ar

### I. INTRODUCTION

The presence of heavy elements in the components of current and planned magnetically confined fusion reactors has prompted interest in the atomic processes affecting highly stripped, high- $Z$  ions. The presence of high- $Z$  impurities causes dilution of the fusion “fuel” in reactors and can strongly affect spatial current distributions and radiative patterns in the plasma. For magnetically confined fusion plasmas, the region between the wall and the last closed flux surface is crucial for its effect on confinement, impurity flux into the plasma, and radiative power losses [1]. Planned fusion devices such as ITER the (International Thermonuclear Experimental Reactor) will achieve temperatures greater than 100 eV near the magnetic last closed flux surface; this energy and momentum must be removed before reaching the reactor’s divertor region [2]. High- $Z$  materials such as molybdenum are being considered as possible candidates for the divertor target material in future fusion reactors in order to minimize the effects of divertor strike plate erosion [3]. In addition, planned schemes for controlling the power to the divertor and for controlling the heat flux onto the divertor strikes plates call for puffing a high- $Z$ , inert gas into the extreme outer part of the plasma in order to form a radiating divertor [3,4]. Thus, understanding the atomic processes that affect the radiation patterns of intermediate charge states of

high- $Z$  atoms is crucial to the development and operation of fusion reactors.

Mo XVI  $E1$  and  $E2$  lines have been observed in the divertor injection tokamak experiment (DITE) [5] and classified by Mansfield *et al.* [6]. Sugar, Reader, and Rowan [7] have recently published improved wavelengths for the Mo XVI  $E2$  lines from observations made in the Texas experimental tokamak (TEXT). In Ref. [7] based on semi-empirical calculations of energy-level values, the authors change one of the classifications made in Ref. [6]. This change is confirmed based on the present *ab initio* calculations for the level structure of the Mo XVI ion. Mo XVI  $E1$  spectral features have been analyzed in a high-density, laser-produced plasma using the unresolved transition array formalism by Klapisch *et al.* [8]. The long lifetime of the upper states of the  $E2$  transitions causes collisional quenching by free electrons at high-electron densities; the absence of  $E2$  lines from Mo XVI is noted in a high-density, laser-produced plasma [9]. “Allowed”  $3d-4p$  lines in the spectrum of Mo XVII have been classified [6,10]. The  $E2$   $3d-4s$  wavelengths in the spectra of Mo XVII to Mo XXIV are to date unknown; except for one identification made below, these lines are predicted to be very difficult to detect.

Models published earlier by Klapisch *et al.* [11] for the density dependence of the  $3d-4s$   $E2$  to  $3d-4p$   $E1$  emission ratio in Mo XV relied on a simple model for the excitation mechanisms feeding the transitions and only a limited set of configurations for radiative cascades into the upper states of the transitions. This paper looks at the analogous ratio in Mo XVI, where we note the following differences: the effect of wave-function mixing on the radiative rates of the  $3d^k-$

\*Department of Physics and Astronomy, The Johns Hopkins University.

†Permanent address: Racah Institute of Physics, The Hebrew University, Jerusalem, Israel.

TABLE I. Configurations used in calculating the level structure and transition rates for Mo XVI.

$3s^23p^63d^9$
$3s^23p^63d^84l(l=s,p,d,f)$
$3s^23p^63d^85l(l=s,p,d,f,g)$
$3s^23p^53d^{10}$
$3s^23p^53d^94l(l=s,p,d,f)$
$3s3p^63d^{10}$

$3d^{k-1}4s$  ( $1 \leq k \leq 9$ ) transitions is studied (Sec. II B), as well as the effect of cascades from highly excited levels into the upper states of the  $E1$  and  $E2$  transitions (Sec. II C). Finally, *ab initio* calculations of collisional transition rates reveal some temperature sensitivity in the  $E2$  to  $E1$  emission ratio for a given ion. We compare our models to observations made in a tokamak plasma (Sec. III) and find good general agreement.

## II. ATOMIC STRUCTURE CALCULATIONS AND COLLISIONAL-RADIATIVE MODELS

### A. Collisional-radiative equations

Collisional-radiative (CR) models for Mo XVI, Mo XVII, and Mo XXIV have been constructed and used to predict the spectral intensity of the  $3d^k-3d^{k-1}4s$  and  $3d^k-3d^{k-1}4p$  transitions for each ion. Line emissivities are calculated by multiplying the total radiative transition rate between levels by the population in the upper level. The level populations are found by solving the set of equations

$$N_j \left\{ \sum_{i < j}^M (A_{ij} + n_e Q_{ij}) + \sum_{k > j}^M n_e Q_{kj} \right\} = \sum_{k > j}^M N_k (A_{jk} + n_e Q_{jk}) + \sum_{i < j}^M N_i n_e Q_{ji} \quad (1)$$

where  $N_j$  is the population of level  $j$ ,  $A_{ij}$  is the radiative decay rate from level  $j$  to level  $i$ ,  $Q_{ij}$  is the collisional rate coefficient (calculated in the distorted-wave approximation [12]) in  $\text{cm}^3/\text{sec}$  from level  $j$  to level  $i$  for excitation or deexcitation, and  $M$  is the number of energy levels considered in the model for a given ion. Atomic structure data and electron collisional excitation rates were generated using the HULLAC package [12,13] of computer programs.

The Lotz formula [14] has been used to generate the collisional ionization rates from both the valence shells and deeply bound subshells of the ground and excited configurations of Mo XV in order to check if these channels for population flux into the excited levels of Mo XVI have any effect on the ratio of the  $3d-4s$   $E2$  to  $3d-4p$   $E1$  emission. We find that ionization channels have minimal effect of the  $E1$  and  $E2$  transitions studied below.

### B. Level structure and wave-function mixing

Mo XVI has 808 levels from the full list of configurations in Table I, and 510 levels when the  $3d^85l$  configurations are excluded. Mo XVI has an energy-level structure with a ground-state doublet,  $^2D_{5/2,3/2}$ , from the  $3p^63d^9$  configura-

tion and several highly populated levels from the  $3p^63d^84s$  configuration (see Sec. II C below) lying between 228 and 251 eV above the ground state. In between these complexes, there exists a doublet from the  $3p^53d^{10}$  configuration,  $^2P_{3/2,1/2}$ , at 163.4 and 181.5 eV [15], respectively, above the ground state. Figure 1 shows the energy-level structure of the  $3d^9$ ,  $3p^53d^{10}$ ,  $3s3p^63d^{10}$ ,  $3d^84s$ , and  $3d^84p$  configurations of Mo XVI. The 45 levels of the  $3d^84p$  configurations are grouped by their total  $J$  values but the precise, relative energy hierarchy of the levels is only suggested. The thick arrows in the figure indicate the  $3d-4s$   $E2$  transitions (short dashes), the  $3d-4p$   $E1$  transitions (solid line), and the two-electron  $E1$  decays between the levels of the  $3d^84s$  and  $3p^53d^{10}$  configurations (long dashes) discussed in the paragraph below.

Recent work by Bauche *et al.* [16] has quantitatively investigated the effects of configuration interaction on the energy levels and transition probabilities of the levels of the  $3d^84s$  and  $3p^53d^{10}$  configurations in Mo XVI. The principal effect on the spectrum of Mo XVI of wave-function mixing between  $3d^84s$  configuration and other configurations that

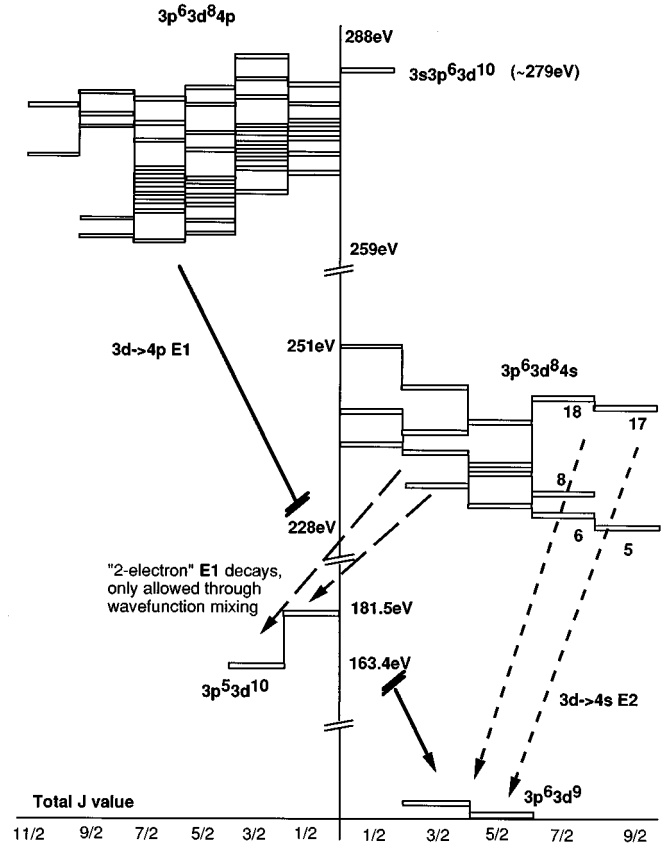


FIG. 1. The energy levels of the  $3d^9$ ,  $3p^53d^{10}$ ,  $3s3p^63d^{10}$ ,  $3d^84s$ , and  $3d^84p$  configurations. The  $3d-4p$   $E1$  (solid lines),  $3d-4s$   $E2$  (short dashes), and “forbidden” two-electron  $E1$  (long dashes) transitions of interest to this work are shown by the thick arrows. The energy axis is not to scale and only suggests the relative position and distribution of levels. The hierarchy of the  $3d^84p$  levels is suggested by the lines at the top of the figure. The numbers near certain  $3d^84s$  levels correspond to the levels discussed in Table III.

TABLE II. Branching ratio for electric quadrupole decays from the  $3d^84s$  levels to the levels of the ground-state doublet in Mo XVI. The numbers in the leftmost column indicate the position in the energy-level hierarchy of the  $3d^84s$  level listed on that line; the  $3d^84s$  levels are listed in order of increasing energy. The numbers in the third column indicate transitions to (1)  $3d^9\ ^2D_{5/2}$  and (2)  $3d^9\ ^2D_{3/2}$ . The fourth column is the branching ratio calculated without the effects of the two-electron transitions to the levels of  $3p^53d^{10}$  discussed in Sec. II B; the last column is the branching ratio that includes the alternative two-electron channels in Sec. II B.

Position	$3d^84s$ level	Final	No mixing	Mixing
5	$(^3F_4, 1/2)_{9/2}$	1	1.00	1.00
6	$(^3F_4, 1/2)_{7/2}$	1	0.96	0.96
		2	0.04	0.04
7	$(^3F_2, 1/2)_{5/2}$	1	0.03	0.02
		2	0.97	0.79
8	$(^3F_3, 1/2)_{7/2}$	1	0.93	0.93
		2	0.07	0.07
9	$(^3F_2, 1/2)_{3/2}$	1	0.78	0.51
		2	0.22	0.14
10	$(^3F_3, 1/2)_{5/2}$	1	0.60	0.54
		2	0.40	0.36
11	$(^3P_2, 1/2)_{5/2}$	1	0.07	0.07
		2	0.93	0.90
12	$(^3P_2, 1/2)_{3/2}$	1	0.99	0.75
		2	0.01	0.00
13	$(^3P_0, 1/2)_{1/2}$	1	0.74	0.51
		2	0.26	0.17
14	$(^3P_1, 1/2)_{3/2}$	1	0.99	0.77
		2	0.01	0.00
15	$(^1D_2, 1/2)_{5/2}$	1	0.22	0.15
		2	0.78	0.57
16	$(^3P_1, 1/2)_{1/2}$	1	0.51	0.43
		2	0.49	0.41
17	$(^1G_4, 1/2)_{9/2}$	1	1.00	1.00
18	$(^1G_4, 1/2)_{7/2}$	1	0.01	0.01
		2	0.99	0.99
19	$(^1D_2, 1/2)_{3/2}$	1	0.32	0.26
		2	0.68	0.54
20	$(^1S_0, 1/2)_{1/2}$	1	0.40	0.04
		2	0.60	0.06

have  $E1$  decays to the levels of the  $3p^53d^{10}$  configuration (and, in like manner, mixing between the  $3p^53d^{10}$  configuration and other configurations that have  $E1$  decays to the levels of the  $3d^84s$  configuration) is to create channels for two-electron  $E1$  decays,  $3p^53d^{10}-3d^84s$ , which compete directly with the  $3d-4s$   $E2$  decays to the ground state [16]. These alternate channels for deexcitation suppress 22 of the 30 possible  $E2$  decays in Mo XVI. Because the  $3d^84s$  levels with  $J=7/2$  and  $J=9/2$  cannot have  $E1$  decays to the  $3p^53d^{10}$  levels (by the  $\Delta J$  dipole selection rule), all observed  $3d^9-3d^84s$   $E2$  lines in Mo XVI originate from these states (see Table I of Ref. [7]). Table II demonstrates the effect of the two-electron decays on the  $3d-4s$   $E2$  lines in Mo XVI. The data in Table II are the branching ratios for  $E2$  transitions toward the ground state (level 1) and the first excited state (level 2) of Mo XVI from the levels of the  $3d^84s$  configuration without the effects of two-electron decays and with the two-electron decays, respectively. For many of the  $3d^84s$  levels, the presence of the two-electron

decays reduces the branching ratio for an  $E2$  transition to the levels of the  $3d^9$  configuration.

Analogous quenching suppresses nearly all of the  $3d^8-3d^74s$   $E2$  transitions in FeI-like Mo XVII. However, there is one level of the  $3d^74s$  configuration that is forbidden from having two-electron  $E1$  decays to the levels of  $3p^53d^9$  (by the  $\Delta J$  dipole selection rule). The maximum  $J$  value for a level from the ground configuration,  $3p^63d^8$ , and also from the  $3p^53d^9$  configuration, is  $J=4$ ; one  $3d^74s$  level obtains the maximum  $J$  value of  $J=6$ ; two-electron  $E1$  transitions to the levels of  $3p^53d^9$  will be forbidden to the  $J=6$  level of the  $3d^74s$  configuration, despite wave-function mixing, by the requirement that  $\Delta J=0, \pm 1$ . CR models indicate that while the ratio of the  $E2$  to  $E1$  emission may be weak for Mo XVII (because of the small number of unquenched  $3d-4s$   $E2$  transitions and the large number of  $3d-4p$   $E1$  transitions that can take place), the individual  $3d-4s$  line, which is not affected by mixing, should be observable. Calculations by RELAC [13] predict that there will be one transition from the

TABLE III. The population of the ground-state doublet and the relative population of upper states of strong  $3d-4s$   $E2$  transitions in Mo XVI at an electron temperature of 200 eV and electron density of  $1.0 \times 10^{20} \text{ m}^{-3}$ . Population in upper states of some of the strong  $3d-4p$   $E1$  transitions is also shown for the sake of comparison. The number for each energy level is that level's position in the energy-level hierarchy; the  $3d^8 4s$  levels are classified as in Ref. [7]; the  $3d^8 4p$  levels are classified as in Ref. [15]. Numbers in brackets represent powers of 10,  $X[Y] = X \times 10^Y$ .

Index	Level	Population	
		4l levels only	5l levels included
1	$3p^6 3d^{9/2} D_{5/2}$	0.100[1]	0.100[1]
2	$3p^6 3d^{9/2} D_{3/2}$	0.533[0]	0.544[0]
5	$3d^8 4s(^3F_4, 1/2)_{9/2}$	0.645[-2]	0.761[-2]
6	$3d^8 4s(^3F_4, 1/2)_{7/2}$	0.325[-3]	0.393[-3]
8	$3d^8 4s(^3F_3, 1/2)_{7/2}$	0.142[-3]	0.175[-3]
17	$3d^8 4s(^1G_4, 1/2)_{9/2}$	0.191[-3]	0.235[-3]
18	$3d^8 4s(^1G_4, 1/2)_{7/2}$	0.135[-3]	0.164[-3]
30	$3d^8 4p(^3F)^2 F_{7/2}$	0.401[-7]	0.414[-7]
31	$3d^8 4p(^3F)^2 D_{5/2}$	0.246[-7]	0.242[-7]
35	$3d^8 4p(^4F)^4 F_{5/2}$	0.278[-7]	0.281[-7]
40	$3d^8 4p(^3F)^2 F_{5/2}$	0.188[-7]	0.185[-7]
44	$3d^8 4p(^3P)^4 D_{7/2}$	0.368[-7]	0.440[-7]
45	$3d^8 4p(^1D)^2 D_{3/2}$	0.126[-7]	0.123[-8]
48	$3d^8 4p(^3P)^2 P_{3/2}$	0.122[-7]	0.128[-7]
51	$3d^8 4p(^1D)^2 P_{3/2}$	0.134[-7]	0.131[-7]
59	$3d^8 4p(^1G)^2 F_{5/2}$	0.173[-7]	0.168[-7]

$jj$ -coupled  $[(3d_{3/2})^3_{j=3/2}(3d_{5/2})^4_{j=4}]_{j=11/2} 4s$   $J=6$  level of Mo XVII to the ground state at a wavelength of 47.456 Å. Examination of the photographic plates from the experiments in TFR (Tokamak Fontenay-aux-Roses) described in Ref. [11] reveal a candidate for this transition at a measured wavelength of 47.474 ( $\pm 0.05$ ) Å. This line was measured in spectra recorded in experiments with molybdenum limiters; the line was absent in spectra taken in the same wavelength region from a vacuum spark-produced plasma. Since in both cases, high- and low-density plasmas, the Mo XVI lines around 45 Å (the Mo XVI  $E1$  lines) are observed, one may assume that the line present only in the low-density (tokamak) plasma is the Mo XVII  $E2$  line.

Calculations in the present work for the possible total angular momentum values of the  $3p^5 3d^{k+1}$  and  $3p^6 3d^{k-1} 4s$  ( $1 \leq k \leq 7$ ) states indicate that all possible  $3d-4s$   $E2$  transitions in charge states Mo XVIII and higher are quenched by the  $3p^5 3d^{k+1} - 3p^6 3d^{k-1} 4s$  two-electron  $E1$  decay channels that arise through wave-function mixing. Mo XVIII ( $k=7$ ), for example, has a maximum  $J$  value for a  $3p^5 3d^8$  level of  $J=11/2$ . The maximum  $J$  value of a  $3d^6 4s$  level is  $J=13/2$ ; all levels of the  $3d^6 4s$  configuration can have  $E1$  decay channels to the  $3p^5 3d^8$  levels created by wave-function mixing. In Mo XIX ( $k=6$ ), the maximal  $J$  value for both a  $3p^5 3d^7$  and a  $3d^5 4s$  level is  $J=7$ . For charge states with ground configurations  $3d^k$  ( $k \leq 5$ ), the maximal  $J$  value for a  $3p^5 3d^{k+1}$  level exceeds the maximal  $J$  value of a  $3d^{k-1} 4s$  level.

### C. Collisional-radiative level populations

The population calculated from Eq. (1) in the  $J=7/2$  and  $9/2$  levels of the  $3d^8 4s$  configuration, relative to the ground-

state population of Mo XVI, is found in Table III. The data in Table III are computed at an electron temperature of 200 eV and a free-electron density of  $1.0 \times 10^{20} \text{ m}^{-3}$ . The first column represents a level's position in the energy-level hierarchy, counting the ground state as one (cf. Fig. 1). The  $3d^8 4s$  levels are named according to the classification in Ref. [7]. The last two columns are the population in a level without any cascades from the  $n=5$  levels (left) and with cascades from the  $n=5$  levels (right). For comparison, Table III also shows the population in some of the  $3d^8 4p$  levels that contribute to the bright  $3d-4p$   $E1$  lines in the model. These levels are named according to their classification in Ref. [15]. Only the  $J=7/2$  and  $9/2$  levels of the  $3d^8 4s$  configuration possess large populations because these levels are forbidden from  $E1$  decays to the ground state by their parity and are forbidden from  $E1$  decays to the  $3p^5 3d^{10}$  doublet, despite mixing with other configurations, by selection rules on  $\Delta J$  and on  $\Delta l$  (see Sec. II B). This accounts for the strong emissivity of the  $E2$  decays from these states.

Table IV shows the calculated  $E2$  decay rates from the  $3d^8 4s$  ( $J=7/2, 9/2$ ) levels and a comparison of observed [7] and calculated  $3d^9-3d^8 4s$   $E2$  transition wavelengths. Table IV also shows the (relative) collisional-radiative intensities for the Mo XVI  $E2$  lines found from Eq. (1). For comparison, some of the strong  $3d-4p$   $E1$  transitions are also listed in Table IV; the observed Mo XVI  $3d^9-3d^8 4p$   $E1$  wavelengths come from Ref. [15]. Figure 2 shows the synthetic emission spectra of Mo XVI and Mo XV at an electron temperature of 200 eV and an electron density of  $1.0 \times 10^{20} \text{ m}^{-3}$ .

TABLE IV. Data on the observed and calculated  $3d-4s$   $E2$  and (some)  $3d-4p$   $E1$  transitions in Mo XVI. The numbers indicating the transition correspond to the levels described in Table III (the initial and final states of the transitions are labeled according to the level indices in Table III). Observed wavelengths for the  $3d-4s$  lines are from Ref. [7]; observed wavelengths for the  $3d-4p$  lines are from Ref. [15]. The wavelength and transition rate calculations are done *ab initio* with RELAC for this paper. CR intensities are from Eq. (1) at an electron temperature of 200 eV and an electron density of  $1.0 \times 10^{20} \text{ m}^{-3}$ . Numbers in brackets represent powers of 10,  $X[Y]=X \times 10^Y$ .

Levels	Observed (Å)	Predicted (Å)	$g_j^* A_{ij}$ ( $\text{sec}^{-1}$ )	CR intensities (arb. units)
		$3p^6 3d^9(5/2)-3d^8 4s(9/2)$		
1-17	51.909	51.723	1.71[8]	37.6
1-5	54.348	54.259	2.46[6]	17.6
		$3p^6 3d^9(5/2)-3d^8 4s(7/2)$		
1-6	54.088	53.988	1.37[8]	62.6
1-8	53.484	53.387	2.04[8]	41.3
		$3p^6 3d^9(3/2)-3d^8 4s(7/2)$		
2-18	52.644	52.392	1.38[8]	26.5
		$3p^6 3d^9(5/2)-3d^8 4p(7/2)$		
1-30	46.859	46.729	5.70[11]	28.4
1-44	45.809	45.848	1.89[12]	100.0
		$3p^6 3d^9(5/2)-3d^8 4p(5/2)$		
1-31	46.841	46.696	1.03[12]	39.8
1-35	46.478	46.381	4.99[11]	22.6
1-40	46.291	46.102	1.05[12]	31.3
		$3p^6 3d^9(5/2)-3d^8 4p(3/2)$		
1-45	46.043	45.828	8.56[11]	25.5
1-51	45.659	45.452	5.67[11]	17.9
		$3p^6 3d^9(3/2)-3d^8 4p(5/2)$		
2-59	45.756	45.535	1.15[12]	31.0
		$3p^6 3d^9(3/2)-3d^8 4p(3/2)$		
2-48	46.043	46.258	9.84[11]	30.4

### III. RESULTS AND DISCUSSION

Mo XVI spectra have been experimentally obtained from the Alcator C-Mod tokamak [17] at the Massachusetts Institute of Technology (MIT). C-Mod has a molybdenum first wall; consequently, molybdenum is the dominant high-Z impurity in the plasma. Additional molybdenum was introduced into the plasma discharge by the laser blow-off technique [18]. The target Alcator C-Mod plasmas were diverted deuterium plasmas with major parameters: plasma current of 0.8 MA, central electron temperature of 1.6–1.7 keV, central electron density of 1.0 to  $2.0 \times 10^{20} \text{ m}^{-3}$ , toroidal magnetic field of 5.4 T, major radius of about 67 cm, and minor radius of about 21 cm.

The molybdenum spectra in the 40 to 55 Å range were obtained using a multilayer mirror (MLM) -based polychromator built and calibrated at the Johns Hopkins University. Details of the instrument have recently appeared elsewhere [19,20]. The polychromator had a view of the plasma through a central radial cord. It monitored the particular

wavelength band of the  $3d-4p$   $E1$  ( $\sim 46.45$  Å) and  $3d-4s$   $E2$  transitions ( $\sim 54.27$  Å) in Mo XVI on successive discharges. Two series of reproducible plasma discharges were run, one with a nominal core electron density of  $1.0 \times 10^{20} \text{ m}^{-3}$  and the other with a nominal core density of  $2.0 \times 10^{20} \text{ m}^{-3}$ .

The ratio of  $E2$  to  $E1$  emission is found from the collisional-radiative models for Mo XVI by

$$R(n_e, T_e) = \frac{\sum_{\text{all } E2 \text{ decays}} I(3d \rightarrow 4s)}{\sum_{\text{all } E1 \text{ decays}} I(3d \rightarrow 4p)}, \quad (2)$$

where  $I(f \rightarrow i)$  is the emissivity of the transition.  $R_0$  is defined as the value of  $R(n_e, T_e)$  at  $n_e = 1.0 \times 10^{19} \text{ m}^{-3}$  for a given  $T_e$ . [ $M1$  and  $M2$  decays are also included in the CR models, but since they are found to have no effect on the emissivity of the  $E2$  transitions, they have no effect on  $R(n_e, T_e)$ ]. In what follows, the observed values of the Mo XVI  $3d-4s$   $E2$  to  $3d-4p$   $E1$  emission ratio are found by

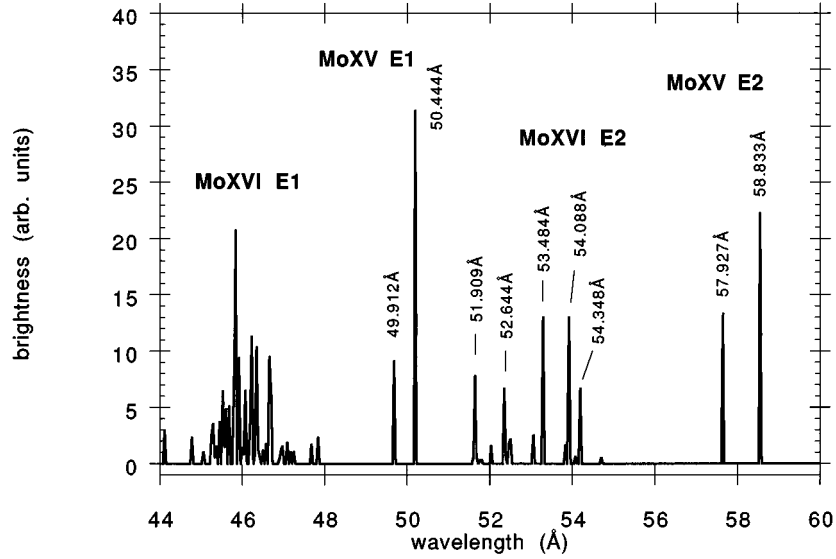


FIG. 2. Synthetic collisional-radiative spectrum in the wavelength range of the *E1* and *E2* transitions considered in the present work. Conditions used in calculating the spectrum are  $T_e = 200$  eV and  $n_e = 1.0 \times 10^{20} \text{ m}^{-3}$ . Wavelengths written above spectral features of Mo xv are from Ref. [11]; wavelengths written above the *E2* features of Mo xvi are from Ref. [7].

integrating in wavelength the area under the (unresolved) peaks formed by each class of transitions in the MLM-recorded spectrum after an appropriate correction for background from other molybdenum charge states has been made.

The data obtained in the current experiments yield a value of  $R(n_e, T_e) = 0.5 \pm 0.15$  for Mo xvi at densities of both  $0.6 \times 10^{20} \text{ m}^{-3}$  and  $1.5 \times 10^{20} \text{ m}^{-3}$ ; the 30% uncertainty in the reported ratios is the total of both the photometric calibration error and that introduced by the shot-to-shot irreproducibility during the wavelength scans. The values of  $R(n_e, T_e)$  obtained from the CR models are listed in Table V. Inclusion of the  $3d^8 5l$  cascades increases the value of  $R(n_e, T_e)$  by 15% at temperatures of 100 eV or less, and by less than 10% at temperatures above 100 eV. The ionization channels from Mo xv change the value of  $R(n_e, T_e)$  by less than 2% at all temperatures. The behavior of  $R(n_e, T_e)$  versus electron density for Mo xvi is shown in Fig. 3.

From models for the collisional-radiative spectrum of Mo xvi, which include all of the  $3d^8 5l$  configurations, the

measured values of  $R(n_e, T_e)$  will obtain in a region of the plasma with an electron temperature between 75 and 150 eV. Calculations and observations for NiI-like ions similar to those described above indicate that the NiI-like Mo xv is found at a temperature near 100 eV. Under ionization equilibrium conditions, the NiI-like ion is expected to exist at an electron temperature near 130 eV, and the CoI-like is expected at an electron temperature slightly above 200 eV. In the present experiments we could not measure the radial distribution of the Mo xv and Mo xvi emissions. Even though the electron-density and temperature profiles are measured, we cannot, therefore, confirm directly the CR modeling predictions. The comparison of the *E1* emission of the NiI- and CoI-like charge states indicates that at higher densities the emission is originating from a region where the electron temperature is about 100 eV. One should remember that in addition to the temperature and density dependence of the ionization and recombination rates, particle transport also affects the charge-state distribution.

TABLE V. The value of  $R(n_e, T_e)$  in Mo xvi at nine different free-electron densities. Numbers in brackets represent powers of 10,  $X[Y] = X \times 10^Y$ .

$n_e(\text{cm}^{-3}) \setminus T_e$ (eV)	50	75	100	150	200	300
1.00[13]	0.840	0.685	0.620	0.564	0.506	0.456
5.00[13]	0.785	0.640	0.606	0.551	0.475	0.429
1.00[14]	0.748	0.602	0.561	0.538	0.450	0.405
5.00[14]	0.539	0.444	0.427	0.414	0.340	0.309
1.00[15]	0.415	0.344	0.327	0.319	0.269	0.245
5.00[15]	0.152	0.127	0.120	0.114	0.105	0.098
1.00[16]	0.085	0.072	0.062	0.061	0.060	0.057
5.00[16]	0.016	0.013	0.013	0.013	0.011	0.011
1.00[17]	0.007	0.006	0.007	0.006	0.005	0.004

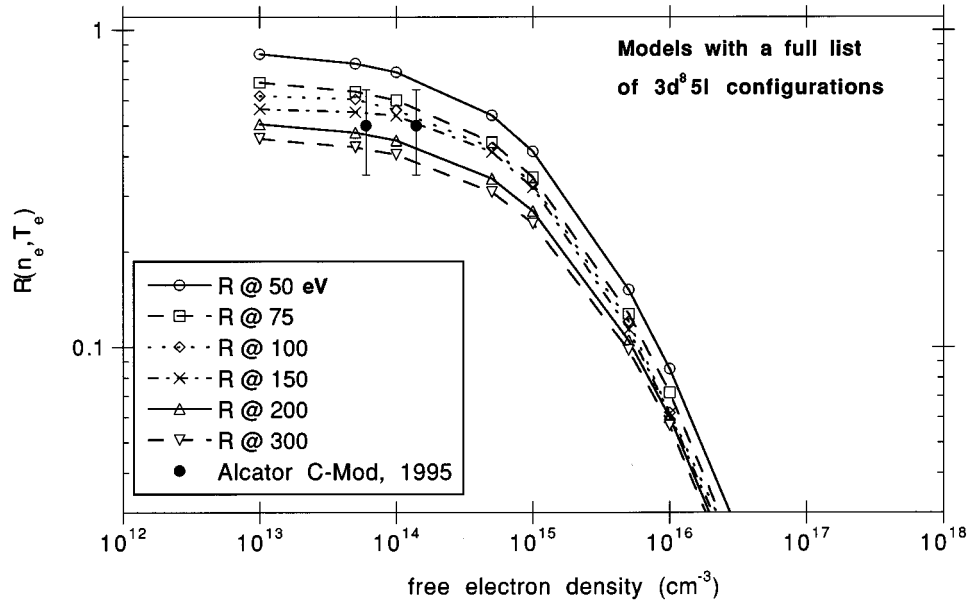


FIG. 3. Plot of  $R(n_e, T_e)$  as a function of density in the coronal regime for Mo XVI showing effects of changes in electron temperature. From top to bottom, the traces are for the  $E2$  to  $E1$  ratio as computed at 50, 75, 100, 150, 200, and 300 eV. All plots are for ratios computed with  $3d^9 5l$  cascades. The solid points are from measurements in the Alcator C-Mod tokamak.

#### IV. CONCLUSIONS

We identify a bright  $3d^8-3d^7 4s$   $E2$  line for Mo XVII at 47.472 Å based on *ab initio* calculations and the behavior of the line in observations made in both low-density (tokamak) and high-density (vacuum spark) plasmas. In the cases where  $E2$  lines are unobserved (all ions Mo XVIII to Mo XXIV), the suppression of the lines is explained by dipole decays to low-lying levels other than the ground state that become allowed through configuration interaction in the  $3d^{k-1} 4s$  states with excited states that have  $E1$  decays to the  $3p^5 3d^{k+1}$  levels (and in like manner, mixing between the  $3p^5 3d^{k+1}$  states and excited configurations that have  $E1$  decays to the  $3d^{k-1} 4s$  levels).

The behavior of the ratio of  $3d-4s$   $E2$  to  $3d-4p$   $E1$  line emission in Mo XVI has been studied as a function of density. The sharp falloff in the value of this ratio for Mo XVI above certain densities provides a plasma diagnostic for planned fusion reactors. The models in the present work for the collisional-radiative emissivity of both  $3d^9-3d^8 4s$   $E2$  and

$3d^9-3d^8 4p$   $E1$  transitions include cascades from  $3d^8 5l$  configurations and the feeding of the upper states of the  $E2$  and  $E1$  transitions by direct impact ionization from Mo XV. The ratio of  $E2$  to  $E1$  emission increases because of the effect of the cascades and is insensitive to the effect of the ionization channels for population flux into and out of the upper state of a transition. Observation made in a high-temperature, low-density tokamak plasma supports the predictions of the models for the  $E2$  to  $E1$  emission ratio in Mo XVI.

#### ACKNOWLEDGMENTS

The authors would like to thank Dr. J. Terry and Dr. J. Rice and all of the staff at the Plasma Fusion Center at MIT for their help with the experiments described in this paper. The present work was performed under the auspices of the U.S. Department of Energy by contract between the Plasma Spectroscopy Group at Johns Hopkins University and the Lawrence Livermore National Laboratories under Contract No. W-7405-ENG-48.

- [1] R. C. Isler, Nucl. Fusion **24**, 1599 (1984); J. Cummings, S. Cohen, R. Hulse, D. Post, M. Redi, and J. Perkins, J. Nucl. Mater. **176&177**, 916 (1990).
- [2] Y. Shimomura, Phys. Plasma **1**, 1612 (1994).
- [3] D. Post, R. Hulse, and D. Stotler, Contrib. Plasma Phys. **34**, 300 (1994).
- [4] S. Allen, M. Rensink, D. Hill, R. Wood, D. Nilson, B. Logan, R. Stambaugh, T. Petrie, G. Staebler, M. Mahdavi, R. Hulse, and R. Campbell, J. Nucl. Mater. **196**, 804 (1992).
- [5] DITE Tokamak Group, in *Proceedings of the 8th European*

*Conference on Controlled Fusion and Plasma Physics* (V. Koepckey, Prague, 1977).

- [6] M. W. D. Mansfield, N. J. Peacock, C. C. Smith, M. G. Hobby, and R. D. Cowan, J. Phys. B **11**, 1521 (1978).
- [7] J. Sugar, J. Reader, and W. Rowan, Phys. Rev. A **51**, 835 (1995).
- [8] M. Klapisch, E. Meroz, P. Mandelbaum, A. Zigler, C. Bauche-Arnoult, and J. Bauche, Phys. Rev. A **25**, 2391 (1982).
- [9] G. Zeng, H. Daido, K. Murai, Y. Kato, M. Nakatsuka, and S. Nakai, J. Appl. Phys. **72**, 3355 (1992).

- [10] J. Wyart, M. Klapisch, J. Schwob, N. Schweitzer, and P. Mandelbaum, *Phys. Scr.* **27**, 275 (1983).
- [11] M. Klapisch, J. Schwob, M. Finkenthal, B. Fraenkel, S. Egert, A. Bar-Shalom, C. Breton, C. DeMichelis, and M. Mattioli, *Phys. Rev. Lett.* **41**, 403 (1978).
- [12] A. Bar-Shalom, M. Klapisch, and J. Oreg, *Phys. Rev. A* **38**, 1773 (1988).
- [13] M. Klapisch, *Comput. Phys. Commun.* **2**, 239 (1971); M. Klapisch, J. L. Schwob, B. S. Fraenkel, and J. Oreg, *J. Opt. Soc. Am.* **67**, 148 (1977).
- [14] W. Lotz, *Z. Phys.* **216**, 241 (1968); **232**, 101 (1970).
- [15] A. Ryabtsev and J. Reader, *J. Opt. Soc. Am.* **72**, 710 (1982).
- [16] J. Bauche, C. Bauche-Arnoult, A. Bachelier, and W. H. Goldstein, *J. Quant. Spectrosc. Radiat. Transfer* **54**, 155 (1995); see also, J. Bauche, C. Bauche-Arnoult, A. Bachelier, K. B. Fournier, and W. H. Goldstein (unpublished).
- [17] I. H. Hutchinson *et al.*, *Phys. Plasmas* **1**, 1511 (1994).
- [18] E. Marmor, J. Cecchi, and S. Cohen, *Rev. Sci. Instrum.* **46**, 1149 (1975).
- [19] M. May, M. Finkenthal, S. Regan, H. W. Moos, J. Terry, M. Graf, K. Fournier, and W. Goldstein, *Rev. Sci. Instrum.* **66**, 561 (1995).
- [20] M. May, A. Zwicker, H. W. Moos, M. Finkenthal, and J. Terry, *Rev. Sci. Instrum.* **63**, 5176 (1992).